ELSEVIER

Journal of Nuclear Materials 317 (2003) 83–92

journal of nuclear materials

www.elsevier.com/locate/jnucmat

Study of gel development during SON68 glass alteration using atomic force microscopy. Comparison with two simplified glasses

N. Donzel [a,*], S. Gin [a], F. Augereau [b], M. Ramonda [c]

[a] CEA Valrhô, DIEC/SESC/LCLT BP17171 30207 Bagnols-sur-Cèze cedex, France

[b] LAIN, UMR 5011, Université Montpellier II, Sciences et Techniques du Languedoc, Place Eugène Battalion 34095, Montpellier cedex 5, France

[c] LMCP, Université Montpellier II, Sciences et Techniques du Languedoc, Place Eugène Battalion 34095, Montpellier cedex 5, France

Received 1 March 2002; accepted 13 December 2002

Abstract

Literature mentions several physicochemical studies concerning the characterisation of the alteration films that are formed during the dissolution of the nuclear glasses. Up to now, however, no study had been undertaken on the evolution of the alteration film thickness by in situ technique. This study proposes to carry out atomic force microscopy (AFM) in liquid and dry conditions in order to measure the shrinkage or swelling of the alteration film. This work is performed on the glass SON68 and on two glasses with simplified compositions. The results obtained reveal a shrinkage of the alteration film for the simplified glasses and, in situ (underwater), a slight swelling for the SON68 glass caused by the formation of crystalline phase (phyllosilicates) on the surface. In all three cases, when alteration progresses, it increases the density of the gel and the volume occupied by the alteration products tends to be equal to the volume initially occupied by the glass (called isovolumetric alteration). Finally, the drying leads to an important shrinkage. These results could be used to evaluate the potential impact of the internal cracks of an industrial glass block.

1. Introduction

In France nuclear glass processing consists of a fusion at high temperature of a mixture of aluminoborosilicate frit glass and of calcine containing the radionuclides. The melted glass is cast in a stainless steel canister and then stored on site. At the time of cooling a high heat gradient is created between the centre and the wall of the block. This creates sufficiently important mechanical stresses to fracture the glass. This fracturing generates an important internal surface that could be leached if water come in.

Dissolution kinetics of nuclear glasses have been extensively studied [10,13]. In the case of the French glass (called R7T7), a gel formation, resulting from in situ recondensation of the hydrolysed species and of crystallised secondary phases was observed. At temperatures lower than 100 °C, these secondary phases are mainly phyllosilicates, which develop at the glass/gel interface [2,14]. According to the conditions in which it is formed, the gel can be considered as a diffusion barrier, which limits the alteration kinetics of the glass [3]. The role of the phyllosilicates remains to be specified. Recently Frugier et al., put forward the idea that the growth of these phases could explain the residual rate observed at high reaction progress [17]. In addition, for the SON68 glass (R7T7 inactive glass reference), Valle has shown that, in an open system, the rate of phyllosilicates growth was approximately 10 times lower than the rate of the gel growth [4].

* Corresponding author. Address: LAMMI, Univ. Montpellier II, Montpellier cedex 05 34095, France.

E-mail address: donzel@univ-montp2.fr (N. Donzel).

0022-3115/03/$ - see front matter © 2003 Elsevier Science B.V. All rights reserved.
doi:10.1016/S0022-3115(02)01705-1

Table 1
Composition of the simplified and SON68 glasses (% mass of oxides)

Glass	SiO_2	Na_2O	B_2O_3	Al_2O_3	CaO	ZrO_2	Ce_2O_3	Li_2O	Other oxides
CJ4	56	13	17	6	5	3			
CJ6	54	11	16	6	5	4	4	2.28	
SON68	45.5	9.9	14	4.9	4	2.6	0.9	2	16.2

For several years the CEA (Commissariat à l'Energie Atomique) has been studying simplified glasses with the aim of identifying the role of the glass components on the gel properties and on the nature of crystalline phases likely to be formed [5–11,15]. In the case of SON68 glass, we could show that calcium played an essential role in the protective gel effect [9,11]. Synergies between Al and Ca or Zr and Ca were also demonstrated in the protective gel effect. Looking at the kinetics, a glass containing seven oxides (SiO_2, B_2O_3, Na_2O, Al_2O_3, CaO, ZrO_2, Ce_2O_3), composed with the same elementary molar ratio as the SON68 reference glass (called CJ6), can be regarded as good model of the nuclear glass [9,11]. Contrary to the SON68 glass, the simplified glass does not develop phyllosilicates during its alteration. This is due to the fact that it contains neither iron nor zinc.

This study aims to determine the alteration film (gel+phyllosilicates) volume formed during the SON68 glass alteration to apprehend the phenomena likely to occur within an industrial block. A swelling of the alteration film could limit the potential impact of these internal cracks, while a shrinkage could lead to a lowering of the ratio between the glass surface and the volume of solution and could increase the potential impact of these cracks. This study is carried out by AFM, which makes it possible an in situ evaluation in volume change by maintaining the samples in water and a shrinkage quantification due to the drying of the samples.

2. Materials and methods

2.1. Composition and density of the glasses

The study is carried out on three glasses, the most complex one being the SON68 glass.

Two simplified glasses called CJ4 and CJ6 respecting the SON68 glass elementary molar ratio were studied. Tables 1 and 2 show the mass compositions and the densities of the studied glasses.

2.2. Glass preparation

The SON68 glass was prepared by fusion of a mixture of phosphates, oxides and carbonates to 1200 °C, using the method described by Pacaud et al. [6]. The glass was then placed in a preheated mould and reheated in a furnace.

Table 2
Density of the studied glasses

Glass	CJ4	CJ6	SON68
ρ_v ($g\,cm^{-3}$)	2.50	2.61	2.75

Table 3
Making simplified glass conditions

Glass	$T_{elaboration}$ (°C)	Refining (h)	$T_{annealing}$ (°C)	Annealing (h)
CJ4	1400	3	530	1
CJ6	1450	3	530	1

The elaboration conditions of all the simplified glasses are summarised in Table 3. The preparation procedure for all the simplified glasses was as previously described for the glass SON68.

A study by Rayleigh–Brillouin light diffusion showed the good homogeneity of these glasses [9]. This technique made it possible to detect crystals or clusters above 50 Å, showed no heterogeneity between these glasses.

2.3. Preparation of glass samples

The glass bars were firstly cut out into coupons of $12 \times 12 \times 2\ mm^3$. Their surfaces were polished using SiC craftpaper up to a grade 4000. Thereafter, we deposited, using Joule effect thermal evaporation, a thin film of chromium on the half of a large face of the coupons followed by a thin film of gold (typically between 100 and 200 nm). The thin film of chromium improves the adherence of the gold layer. The sample was heated to 250 °C in a vacuum tank maintained between 5×10^{-5} and 10^{-6} Torr.

The thickness of the deposit was checked ex situ using a quartz microbalance and is also measured in situ using AFM. The gold layer defined then a reference in the vertical axis. As a result of its sealing abilities, this layer provided a protection for the alteration, making it possible to evaluate the shrinkage or swelling of alteration films by measuring the difference in height between the surface of the deposits and the altered surface. The

sealing of the gold layer was checked after the alteration test by SEM.

2.4. The leaching procedure

A solution of KOH (pH 9) was used for leaching the glasses. pH has not been measured during experiments. SON68 and simplified glasses have been widely studied [9] and if we consider glass composition (simplified glasses present the same stoichiometry than SON 68 glass and therefore the same B/alkaline ratio which is correlated to pH values) pH is quickly buffered to 9 ($pKaB[OH]_3/B[OH]_4^-$). So we consider for all experiments that pH values are similar. Concerning the leachant, secondary phases which precipitate are phyllosilicates and nature of these phases depends, among other parameters, on the composition of the solution. CEA studies have shown that phyllosilicate composition was not correlated on the properties and on the nature of the gel. Consequently, the same results are expected experimenting with NaOH, KOH or H_2O as leachant solution. Teflon containers of 120 ml were used as reactors. The amount of solution introduced into the reactor was adjusted according to the reactive glass surface in order to preserve a S/V ratio equal to 0.7 cm^{-1} (S/V corresponds to the ratio between the reactive surface of the glass coupons and the volume of the leachate).

Prior to leaching, the glass coupons were washed with acetone using ultrasonic bath then rinsed with distilled water. The samples were placed on supports in Teflon and were introduced into a reactor and placed in the oven at 90 °C. After each time duration, a glass coupon was removed, approximately 5 ml of solution was taken to maintain a constant S/V ratio. A fraction of the taken volume is used to keep the face of the monolithic sample wet for AFM characterization. The remaining fraction of the solution is filtered at 0.45 μm, acidified (HNO_3, 0.5N) and then analysed by ICP-AES. After characterization by AFM, the glass sample is dried in air at 30 °C and then characterized again by this technique.

2.5. ICP-AES solution analysis

This method of analysis is used to measure the concentration of the elements Si, B, Na in the leachates. Accuracy of these measurements ranges between 3% and 5%.

From these concentrations, the normalised mass loss calculated for the element i can then be calculated using the following formula:

$$NL_i = \frac{C_i}{X_i \frac{S}{V}}$$

with C_i as the concentration ($mg\,l^{-1}$) of the ith element in the solution and X_i the mass fraction of the ith element within the glass. The NL_i value (expressed in $g_{glass}\,m^{-2}$) allowed us to measure the quantity of altered glass calculated from tracer elements of alteration. In the studied glasses, boron constitutes an alteration tracer element because it is a glass network former and is not retained in the alteration product [16].

Thus, the alteration thickness (expressed in μm) can be calculated using the glass density ρ ($g\,cm^{-3}$):

$$A_{th} = \frac{NL(B)}{\rho}.$$

The retention factor, F_i, of the ith element in the glass alteration products is defined by the following relation:

$$F_i = 1 - \frac{NL_i}{NL_B}.$$

2.6. AFM measuring principle

The AFM equipment used for this study is a 'Dimension 3100 Nanoscope IIIa' of Digital Instruments equipped with a liquid cell. The Si_3N_4 tips used in this study have a curvature radius of 20 nm and have a Young modulus of 140 GPa. The underwater measurements are carried out in contact mode with triangular cantilever which have a stiffness constant $k = 0.06$ N/m. Measurements on dried samples are carried out in intermittent contact mode (also called tapping mode) with stiffness constant cantilevers $k = 40$ N/m. The image acquisition is realised by controlling the deflection. This parameter is maintained constant during (x, y) displacement and is detected via an optical system. The size image ranges between 250×250 nm^2 and 80×80 μm^2, 512×512 points obtained to a scanning frequency ranging between 0.4 and 2 Hz.

The height variation measurements in the z-axis and the surface roughness σ_{RMS} (root mean square) are determined by Nanoscope 3 software.

In order to measure correctly the shrinkage or swelling of the alteration film, the AFM probe must be placed in an homogeneous environment and free from pollution. To achieve this, a systematic observation of the quality of the sample surface is carried out using an optical camera coupled with the (x, y) displacement table. This created the best conditions, which made it possible to take an image of an isolated area of the gold layer and the altered glass area. Fig. 1 shows the transition between gold and glass where the measurement of the thickness of the layer before leaching could then be taken.

The same measurement is then made on all the samples after leaching in liquid and dry condition.

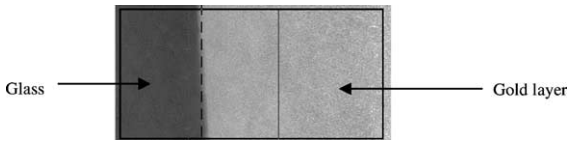

Fig. 1. AFM image of the gold–glass transition aera before leaching.

3. Results and discussion

3.1. Surface qualities and reliability of measurements

3.1.1. Characteristics of the gold deposit

To ensure that differences in height between the gold film and the altered glass surface was correct, it is necessary to study their surface qualities and in particular to quantify their roughness [7,8]. Several images, under the various operating conditions, were taken of both areas and on the various types of sample. The imagery associated with statistical data processing makes it possible to measure standard deviation to the average distribution of the heights (roughness) of the various present structures (σ_{RMS}).

$\sigma_{\mathrm{RMS}} = \sqrt{\sum_i \frac{(Z_i - \langle Z \rangle)^2}{N}}$, with Z height defined for any point (x, y), $\langle Z \rangle$ heights average and N the number of points.

We point out that the roughness of the gold layer does not exceed 2 nm and that the only defects appearing on golden surface are impurities coming likely from the leachate. This pollution does not effect the quality of the measurements as we saw previously how to solve this problem.

3.1.2. Study of the roughness

The surface analysis of the various altered samples shows a difference in roughness between the gels observed in dry condition and the gel observed in liquid condition. This can be seen looking at two images of 260×260 nm^2 showing the alteration layer maintained in a liquid condition (Fig. 2(a)) and dried in air, (Fig. 2(b)) as well as two roughness profiles.

The gel reveals a topology characterised by nodules of various size. These nodules are appreciably larger in a

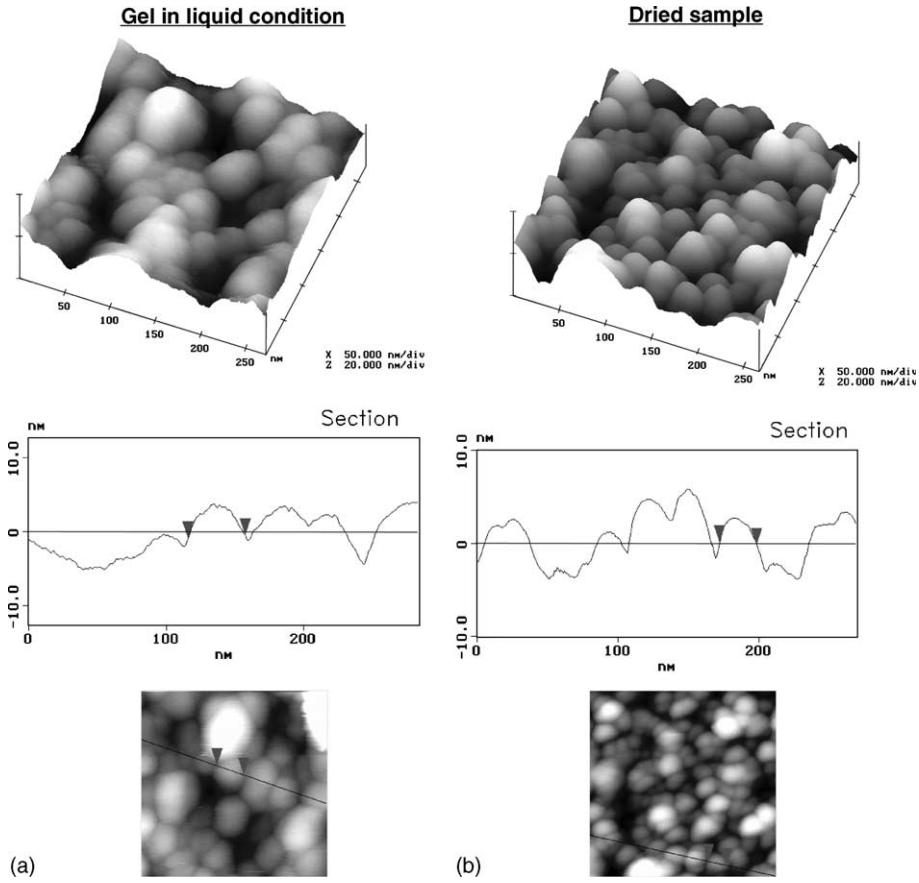

Fig. 2. Relief image and profile of a line of the alteration layer maintained in a liquid condition (a) and after drying of the sample (b).

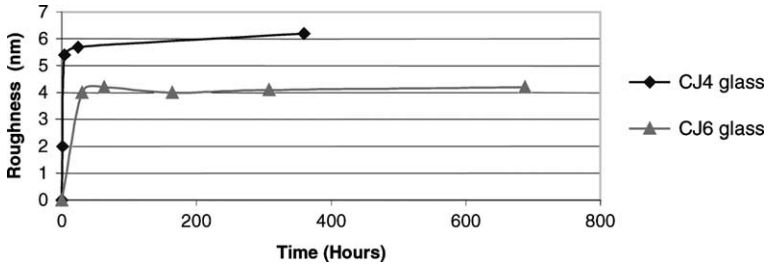

Fig. 3. Roughness evolution of the gel formed on the CJ4 and CJ6 glasses during leaching. Dried samples.

liquid condition than in a dry condition. This difference illustrates the shrinkage involved by the dehydration of the sample. This shrinkage is also visible on the two profiles where the nodule side extension is plotted. For the dried sample a much rougher profile is observed than that seen for the wet sample.

A study of the surface roughness of the gel that resulted during leaching was carried out on the various samples. We give the results obtained for the CJ4 and CJ6 glass samples. In this case gels were dried in air (Fig. 3).

For these two glasses, a rapid increase of the roughness between 0 and 50 hours is noted before reaching a plateau. The plateau shows a noticeable deceleration with the textural development of gel surface. The maximum roughness values reached in a dry condition for the various glass samples are given in Table 4.

The maximum roughness of the SON68 glass in liquid and dryness conditions are much higher than the values found for the simplified glasses (Table 4). This difference is due to the presence of crystalline phases on the nuclear glass surface (Fig. 4). This AFM image reveals the presence of crystalline phases which are phyllosilicates as it was previously demonstrated by Deruelle [3]. In addition, Advocat had shown that phyllosilicates were precipitating at the first stage of the glass alteration [1]. The information of gel morphology is then masked by the presence of the phyllosilicates.

It is important to note that the roughness will not effect the accuracy of height differential measurement since those are obtained averaging of the variations in z of the different lines constituting the image of the gold–glass transition.

Table 4
Maximum roughness values reached at the major limits from the measurements carried out on wet and dried samples

Samples	CJ4	CJ6	SON68
σ_{max} (nm) liquid condition	4	2	50
σ_{max} (nm) dry condition	6	4	100

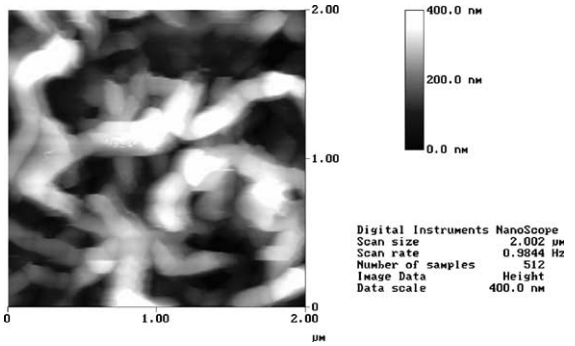

Fig. 4. Relief image of the SON68 glass surface. The image shows the presence of crystallised phases (phyllosilicates).

3.1.3. The phenomenon of indentation, the approach and shrinkage curve

The mechanism of contact between tip and sample surface in the absence of displacement can be clarified using a force–distance curve (approach and shrinkage curve) when the sample is approached and moved away of it. Fig. 5 shows an force–distance curve obtained from the glasses in liquid conditions.

When probe and sample are sufficiently distant so as not to interact there is no deflection (part AB). Then

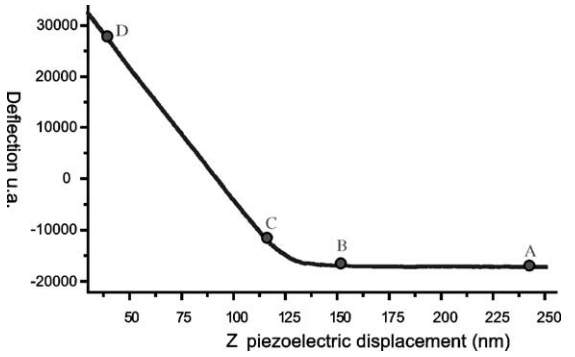

Fig. 5. Force–distance curve reflecting the cantilever deflexion according to the displacement of the piezoelectric ceramic.

when the AFM tip comes into contact with the sample surface, it either meets an infinitely hard material and the deflection then increases linearly with the displacement of the ceramics (part CD). When the AFM tip meets a material of low hardness we observe a curvilinear intermediate area (part BC) which enables us to define an indentation length intrinsic of the studied material (noted thereafter δ). This phenomenon of indentation has always been observed with wet samples. It then becomes necessary to take into account into this length at the time of measuring the shrinkage or swelling, since it tends to over-estimate the difference in height.

3.2. Solution analysis results

The solutions analysis results for the static test carried out with a S/V of 0.7 cm^{-1} are presented in Table 5.

Fig. 6 gives the evolution of the glass alteration thickness (A_{th} in μm) calculated from the boron normalised mass loss.

From a general point of view, the glass dissolution rate depends on its composition, on the temperature, on the pH and on the more or less protective effect of the gel [10]. In the alteration conditions of the study, the kinetics are shown to be almost linear (Fig. 6) and the measured rates approximate to $r_0/10$ by considering the initial speed values given to 90 °C and pH 9 by Gin [11]. As expected, the CJ6 glass presented the same alteration kinetics as that of the SON68 glass, and the CJ4 glass altered more quickly; this difference being due to the fact that the gel formed on this glass is less protective because of the absence of reticulating elements like Zr and Ce.

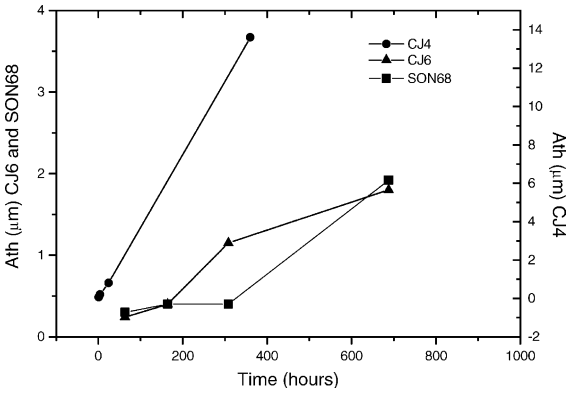

Fig. 6. Evolution of the alteration thickness of the three studied glasses during leaching.

3.3. Results of the AFM measurements

AFM measurements show that the differences between the two areas (covered surface and altered surface) can be measured and the dynamics of the alteration of various studied glasses can be quantified. For example, Fig. 7 shows a 80×20 μm^2 topography image and a profile obtained by averaging the whole set of image lines.

Fig. 8 shows the nomenclature used for the differential heights measurements.

ΔZ_0 (nm) corresponds to the thickness of the gold layer, ΔZ_1 and ΔZ_2 correspond respectively to the differentials in height in a dry and liquid condition.

We define e_1, e_2, e_s, r_1, r_2 by the following: e_1, the underwater shrinkage: $e_1 = \Delta Z_1 - \Delta Z_0 - \delta$ (nm); δ, intrinsic indentation length of the material (nm); e_2, the

Table 5
Results of the analysis of solutions of the three studied glasses for a static test carried out to 90 °C, pH 9, and S/V 0.7 cm^{-1}

Glass	Time (h)	$C(B)$ mg l^{-1}	$NL(B)$ g m^{-2}	C(Si) mg l^{-1}	NL(Si) g m^{-2}	F_{Si}	A_{th} (μm)
CJ4							
	1	0.2	0.05	2.8	0.15	–	0.06[a]
	4	1.9	0.5	11.3	0.61	–	0.2
	24	7.8	2.07	34.3	1.87	0.10	0.8
	360	131	34	198	10.8	0.68	13.6
CJ6							
	63	2.2	0.62	5.8	0.34	0.43	0.24
	164	3.6	1.02	14.3	0.83	0.19	0.4
	308	10.6	3.0	17.8	1.03	0.66	1.15
	688	16.9	4.8	40.1	2.33	0.52	1.8
	1872	40.0	11.3	72.6	4.21	0.63	4.3
SON68							
	63	3	0.99	7.4	0.49	0.50	0.3
	308	3.2	1.05	8.7	0.58	0.44	0.4
	688	16.1	5.25	49.9	3.35	0.36	1.92

[a] The A_{th} value concerning the CJ4 glass for 1 leaching hour was calculated from the normalised mass loss in silicon.

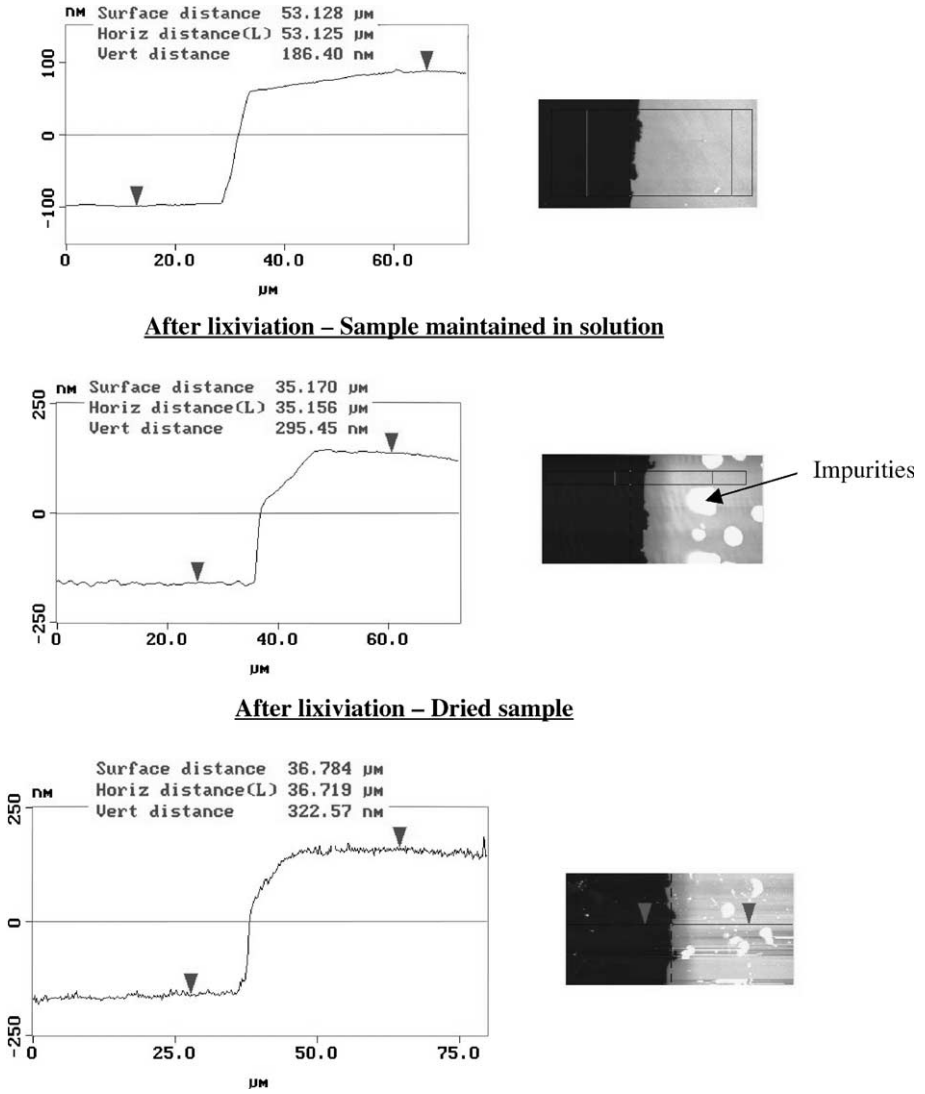

Fig. 7. Relief image and profile obtained by AFM (CJ4 glass).

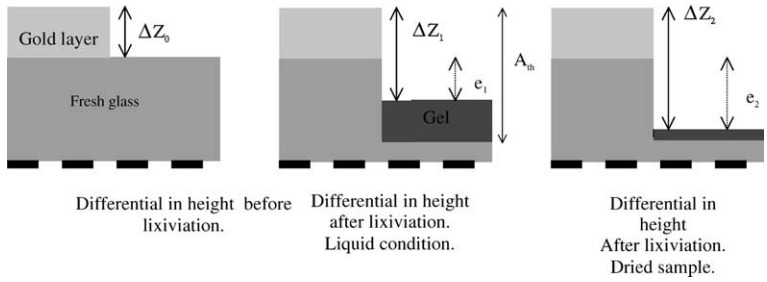

Fig. 8. Diagram showing the nomenclature used.

total shrinkage after drying: $e_2 = \Delta Z_2 - \Delta Z_0$ (nm); e_s, the shrinkage due to drying: $e_s = e_2 - e_1$ (nm).

Note that a negative e_1 corresponds to a swelling of the film. r_1, the relative shrinkage in liquid conditions:

Table 6
Calculations from AFM measurements, glass CJ4

Time (h)	δ (nm)	e_1 (nm)	e_2 (nm)	e_s (nm)	r_1	r_2
0	0	0	0	0	0	0
1	134	30	56	26	0.5	0.43
4	25	59	134	75	0.30	0.37
24	14	95	136	41	0.12	0.05
360	51	550	669	119	0.04	0.008

Table 7
Calculations from AFM measurements, glass CJ6

Time (h)	δ (nm)	e_1 (nm)	e_2 (nm)	e_s (nm)	r_1	r_2
0	0	0	0	0	0	0
63	56	107	226	119	0.45	0.5
164	19	361	430	69	0.90	0.17
308	37	101	499	388	0.09	0.34
688	75	25	580	555	0.014	0.30

Table 8
Calculations from AFM measurements. Glass SON68

Time (h)	δ	e_1 (nm)	e_2 (nm)	e_s (nm)	r_1	r_2
0	0	0	0	0	0	0
63	51	−115	124	239	−0.38	0.41
160	92	−53	131	184	–	–
308	37	−126	146	272	−0.32	0.37
688	–	−116	140	256	−0.06	0.07

$r_1 = e_1/A_{th}$; r_2, the relative shrinkage of the gel due to drying: $r_2 = e_s/A_{th}$.

Tables 6–8 gather the main data resulting from the measurements:

The measurements of height differential present absolute uncertainty of approximately ±5 nm in a liquid condition (uncertainty is primarily due to the operating mode of the AFM in this type of medium). In dry condition, absolute error is lower, about ±2 nm, since measurement is done under less drastic conditions. These values enable us therefore to define in a sufficiently precise way, the variation of the relative shrinkage of the wet gel (Figs. 9(a), 10(a) and 11(a)) and after drying (Figs. 9(b), 10(b) and 11(b)).

Firstly let us compare the data resulting from the underwater measurements. The curves obtained for the two simplified glasses are rather similar. There is a large shrinking of the gel during the first stages of alteration. As the reaction progresses, alteration tends to become isovolumetric. For the SON68 glass, the opposite is observed. The volume occupied by the alteration products (gel+phyllosilicates) is higher than the volume oc-

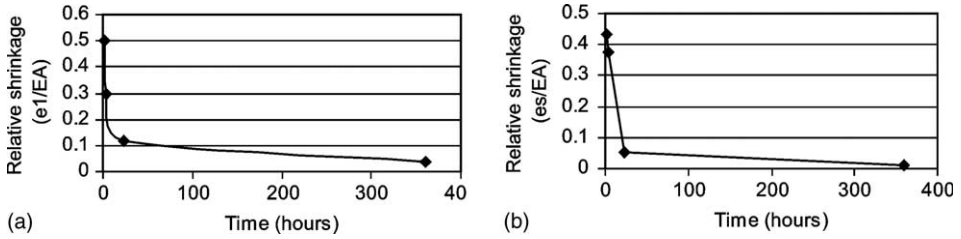

Fig. 9. Evolution of the real relative shrinkage of the wet CJ4 glass sample (a) and of the shrinkage due to drying (b).

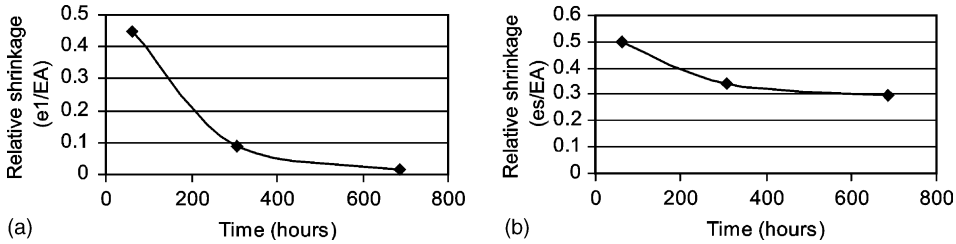

Fig. 10. Evolution of the real relative shrinkage of the wet CJ6 glass sample (a) and of the shrinkage due to drying (b).

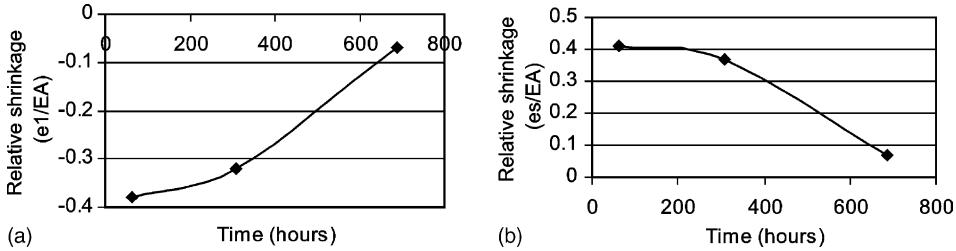

Fig. 11. Evolution of the real relative shrinkage of the wet SON68 glass sample (a) and evolution of the shrinkage due to drying (b).

cupied initially by the glass (up to 40%). When the reaction progresses, it also tends to become isovolumetric. Studies carried out on this glass in diluted conditions (measurements of initial rates) has clearly demonstrated that precipitation of phyllosilicates occurs during the first stages of the glass alteration [12]. Also, by comparing the results obtained on the glass SON68 with those obtained on the CJ6 glass (same alteration kinetics, volume expansion for the nuclear glass and shrinkage for the simplified glass) and considering that the CJ6 glass does not develop phyllosilicates, it can be concluded that the swelling of the nuclear glass is due to the phyllosilicates formation. The main reason explaining why we can observe phyllosilicates on SON68 and not on CJ6 is the glass composition. In fact, the presence of different elements as Fe and Zn seems to be essential to the phyllosilicate formation on SON68 glass. Both elements are absent from CJ6 glass. In addition, these phases are formed at the first stage of the glass alteration essentially because solution is quickly saturated compared with these kind of phases. To make sure that that these phases are developed at the beginning of the alteration glass, we can look at the geochemical modelling proposed in the Advocat thesis [2]. The fact that the volume swelling of the alteration film of the SON68 glass is not maintained in time can be explained by considering that in these conditions the gel grows more quickly than the phyllosilicates. From the work performed by Valle, it can be shown that in these conditions the growth rate of the phyllosilicates is approximately 10 times lower than growth rate of the gel [4].

Now let us consider the shrinkage of dried samples. It can be noted in Figs. 9(b), 10(b) and 11(b) that this shrinkage is very important since it can represent up to 50% of the altered glass thickness. It is also noted that for the three glasses the shrinkage due to drying decreases with time which agrees with the fact that the gel densifies during this time, and this contributes to decreasing its porosity. Concerning the protecting effect of phyllosilicate phases, we can notice that pore sizes are very different: gel shows pore size of a few nanometers while phyllosilicates present several hundred nanometers chink size. Therefore transport properties have to be very different.

3.4. Observation under the scanning electron microscope

In order to check the consistency of the results, a study was carried out by scanning electron microscopy (SEM). The method is destructive and requires a relatively long and meticulous preparation of the sample: cutting, coating in a resin and polishing without damage neither the gel nor the gold layer. Fig. 12 shows a SEM image of the CJ6 glass altered over 688 h. On the left, the homogeneous area represents the glass, on the right an area of equivalent dimension represents resin and between the two at the top of the image, a bright area indicates the gold layer gold which has a strong electronic contrast. In the lower centre of the image, it can be observed that the gel is of uniform thickness. It is important to note that the gel layer increased by approximately 10 μm under gold surface. This alteration

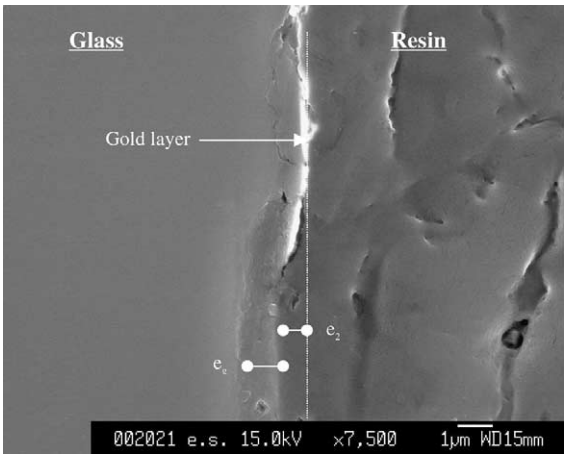

Fig. 12. Observation of the real shrinkage e_2 and of the thickness of the gel in dry condition by scanning electron microscopy. Glass CJ6 altered 688 h.

leads to the formation of a transition area from 10 to 15 μm between the non-disturbed gold layer and the gel. This transition distance is reasonably visible on the AFM profiles (Fig. 7).

The SEM measurements of the gel thickness and of the shrinkage, although not very precise, corresponds to the values obtained by AFM. Thus, for this CJ6 glass sample lixiviated for 688 hours we find by AFM a shrinkage of 580 nm (±5 nm) and a corresponding gel thickness ($e_g = A_{th} - e_2$) of 1200 nm (±10 nm). The SEM image gives respectively for these two values 600 nm (±100 nm) and 1100 nm (±100 nm). The conditions of preparation, the weak precision of the measurements and especially the impossibility of working underwater led us to use this method on only few samples.

4. Conclusion

This study shows the advantages of AFM for the characterisation of morphological surface (precision of the measurements, studies in situ). The measurements carried out make it possible to identify important initial swelling of the alteration film formed on the glass SON68, this swelling being then inclined to decrease in time. The comparison of the results between the SON68 glass and the CJ6 glass shows that the swelling observed on the nuclear glass is likely due to the layer of phyllosilicates. This result suggests that within the internal cracks of an industrial block, the transport of the species in the liquid phase could be limited by the initial volume swelling of the alteration film. Specific experiments will have to be carried out to confirm this result. On the basis of this work, it can be considered in the calculations that no volume change during alteration of the SON68 glass. To be definitive, this conclusion has to be checked at high reaction progress.

References

[1] O. Zarembowitch Deruelle, PhD thesis, Université de Paris, France, 1997.
[2] J. Caurel, PhD thesis, Université de Poitiers, France, 1990.
[3] S. Gin, I. Ribet, M. Couillard, J. Nucl. Mater. 298 (2001) 1.
[4] N. Valle, PhD thesis, INPL Nancy, France, 2000.
[5] S. Ricol, PhD Thesis, Universitée Pierre et Marie Curie, Paris VI, France, 1995.
[6] F. Pacaud, N. Jacquet-Francillon, N. Terki, C. Fillet, Mater. Res. Soc. Symp. Proc. 127 (1989) 105.
[7] Ph. Dumas et al., Europhys. Lett. 22 (1993) 717.
[8] C.F. Quate, Surf. Sci. 299&300 (1994) 980.
[9] C. Jégou, PhD thesis, Université de Montpellier, France, 1998.
[10] E. Vernaz, J.L. Dussossoy, Appl. Geochem. Suppl. 7 (1992) 13.
[11] S. Gin, International Conference Water Rock Interactions, Villasimius, Italy, 10–15 July 2001, p. 219.
[12] T. Advocat, J.L. Crovisier, E. Vernaz, H. Charpentier, Mater. Res. Soc. Scientific Basis for Nuclear Waste management XXIV, Sydney, 27–31 August 2000.
[13] E. Vernaz, S. Gin, C. Jégou, I. Ribet, J. Nucl. Mater. 280 (2000) 216.
[14] S. Gin, E. Vernaz Mater. Res. Soc. Scientific Basis for Nuclear Waste Management XXIV, Sydney, 27–31 August 2000.
[15] C. Jégou, S. Gin, F. Larché, J. Nucl. Mater. 280 (2000) 216.
[16] B.E. Scheetz, W.P.D.K. Freeborn, C. Anderson, M. Zolensky, W.B. White, Mater. Res. Soc. Symp. Proc. 44 (1985) 129.
[17] P. Frugier, I. Ribet, T. Advocat, International Conference ICEM, 30 October 2001, Bruges, Belgium.